Experimental studies of plasma sheath near meshes of different transmissivity*

Li Yi-Ren(李毅人), Ma Jin-Xiu(马锦秀)†, Zheng Yao-Bang(郑尧邦), and Zhang Wen-Gui(张文贵)

Key Laboratory of Basic Plasma Physics and Center for Magnetic Fusion Theory, Chinese Academy of Sciences, and Department of Modern Physics, University of Science and Technology of China, Hefei 230026, China

(Received 25 December 2009; revised manuscript received 5 February 2010)

The measurements of the potential distributions in the boundary layer near meshes with different mesh spacing were conducted in weakly collisional plasmas using a fine-structured emissive probe and the results of the sheath thickness and electric field at the sheath-presheath edge were compared with theoretical models of collisional presheath and collisionless sheath. It was shown that, because the meshes are partially transparent to ions, the sheath is thinner and the electric field is stronger for the mesh of higher transmissivity, owing to the increased ion density in the sheath contributed from the ions transmitted from the other side of the mesh. However, the potential profiles in the presheath remain almost the same for different meshes except for the shift of the sheath-presheath edge. The thickness of the sheath decreases while the electric field at the edge increases with the increase of the neutral gas pressure. Furthermore, depending on the pressure, the measured electric fields at the edge are close to that from the models of a transition region.

Keywords: plasma sheath, presheath, mesh, emissive probe

PACC: 5240K, 5270D

1. Introduction

Close to a wall or any surface in contact with plasma, a nonneutral sheath region forms across which electron and ion densities no longer balance. Next to the sheath is a quasineutral presheath region which connects the sheath to bulk plasma. The plasma-wall transition is one of the classical problems in plasma physics and has received extensive investigations since the time of Langmuir.[1−5] Because of the fundamental importance in plasma-material processing and electrostatic probes as well as in plasma-wall interactions of magnetic fusion devices, the plasma sheath and presheath have attracted much interest in recent years.[6−28]

The sheath is a narrow region with thicknesses on the order of a few electron Debye lengths $\lambda_{\rm D}$ depending on the bias on the wall. The length of the presheath is of the order of the minor of ion collision mean-free-pass $\lambda_{\rm i}$ and plasma extent L depending on neutral gas pressure. It is well known that at the sheath-presheath edge (hereafter termed Bohm sheath edge) the ion velocity must exceed the Bohm velocity (ion-acoustic-speed)[29] $u_{\rm B} = c_{\rm s} = (T_{\rm e}/m_{\rm i})^{1/2}$, where $T_{\rm e}$ and $m_{\rm i}$ are electron temperature and ion mass, respectively. It is also well known that the quasineutral presheath equations yield the discontinuity of the electric field and plasma density gradient at the Bohm sheath edge.[4] In order to overcome this difficulty, Riemann[6] proposed a transition region between the presheath and sheath with a characteristic length on the order of $\lambda_{\rm Ds}^{4/5}\lambda_{\rm i}^{1/5}$ and a characteristic electric field $T_{\rm e}/e\lambda_{\rm Ds}^{3/5}\lambda_{\rm i}^{2/5}$, where the electron Debye length $\lambda_{\rm Ds}$ is evaluated at the sheath edge.

The sheath and presheath have been widely explored theoretically in different depths and in diverse areas of plasma physics but there still remain open questions.[22−28] However, experimental diagnostics are rather rare owing to the difficulties of accurate measurement without significant disturbances to the sheath. Up to now, only two practical diagnostics techniques have been applied to measure the sheath, one using laser-induced fluorescence (LIF) to measure the ion velocity distribution function[30−32] and the other using an emissive probe to directly measure the potential distribution,[33] though some other

*Project supported by the National Natural Science Foundation of China (Grant Nos. 10875121 and 40831062), partially by CAS Knowledge Innovation Program (Grant No. kjcx2-yw-n28), and the National Basic Research Program of China (Grant Nos. 2008CB717800 and 2009GB105001).

†Corresponding author. E-mail: jxma@ustc.edu.cn

© 2010 Chinese Physical Society and IOP Publishing Ltd

techniques have also been proposed.[34−36] It was experimentally shown that the potential distribution in the sheath is in agreement with Riemann's transition region model,[33] but other properties have not been verified.

Previous investigations on the plasma-wall transition were for the case of totally absorbing walls. In laboratory devices, however, partially transparent meshes were often introduced into plasmas to control the plasma parameters or launch collective waves.[37−41] Such a process depends sensitively on the boundary structure near the meshes. It often happens that the size of the spatial grid is less than the Debye length and sheath thickness for laboratory tenuous plasmas. Thus, an overall smooth sheath forms around the meshes except the region very close to the wires of the meshes. Obviously, the sheath structure near the partially transparent walls is quite different from that near the totally absorbing walls. In a previous work, we measured the potential profiles near a metal plate and a mesh and found that the sheath region is much thinner in the case of the mesh than that of the plate.[42] However, the detailed structures of the boundary layer near the meshes need further investigations.

This paper presents the experimental studies on the sheath and presheath structures near negatively biased meshes with different grid spacing immersed in a weakly collisional plasma in a modified double-plasma device. The experimental arrangement is described in Section 2. The measured potential distributions and the electric fields at the sheath-presheath edge and the comparison with theoretical models are presented in Section 3. The main conclusions are summarized in Section 4.

2. Experimental arrangement

The experiment was conducted in a modified double-plasma device,[43] which consists of two identical grounded chambers each 500 mm long and 500 mm in diameter, as schematically shown in Fig. 1. The plasma was generated in the source region by the discharge between hot filaments and anode mesh and diffused through a separation grid (SG, 440 mm in diameter, 3.15 lines/mm, grounded) into the experimental region. The plasma parameters in the experimental region measured by a cylindrical probe (CP) were: electron density n_e a few times of 10^8 cm^{-3} and temperature T_e around 1–2 eV. The ion temperature was close to room temperature.

In the experiment, the separation grid was located near the anode and filaments to enlarge the experimental region. Three small meshes with same diameter (94 mm) but different mesh spacing (M1: 0.79, M2: 3.15, and M3: 4.33 lines per millimeter, the corresponding geometrical transmissivities are 80%, 60%, and 50%, respectively) were mounted in the right chamber. The negatively biased meshes were placed near the centre of the right chamber one after another, where the potential profiles around each mesh were measured by an emissive probe (EP). When the sheath around one of the meshes was measured, the other two meshes were moved to near the end wall or side wall of the chamber to minimize their disturbance to the plasma. The emissive probe was made of tungsten wire 6 mm in emitting length and 0.025 mm in diameter. The detailed structure can be found in Ref. [42].

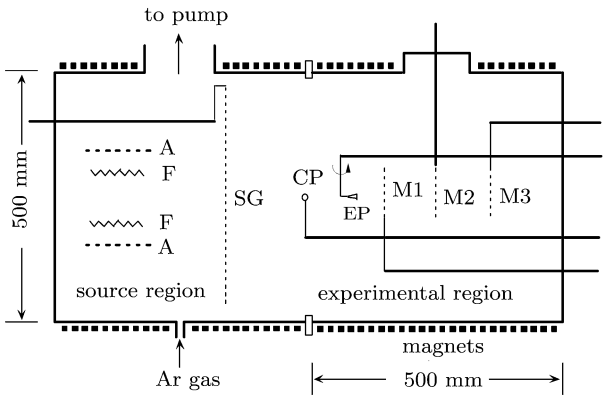


Fig. 1. Schematic diagram of the experimental setup. The symbols denote A: anode, F: filament, SG: separation grid, CP: cylindrical probe, EP: emissive probe, and M1, M2, M3: small meshes with grid spacing 0.79, 3.15, and 4.33 lines per milimeter, respectively.

The movement of the emissive probe was controlled by a ballscrew and the displacement was accurately determined by a vernier scale bound to the probe rod and sliding on a fixed ruler.[42] The plasma potential V was obtained by the inflection point method of the I–V curve of the emissive probe in the limit of zero-emission,[44,45] which is the extrapolation of the curve of V versus emission current to the point of zero emission current.

The pressure of the Ar gas was in the range of 3.6×10^{-2}–1.5×10^{-1} Pa. Since the ion collisions are mainly due to the charge-exchange collisions with Ar atoms, the cross section σ is of the order of

6×10^{-15} cm^2.[43,46] Thus, the ion mean-free-path is in the range of $\lambda_i \sim 51$–213 mm. In addition, the electron Debye length in the bulk plasma is $\lambda_D \sim 1$ mm. Therefore, the experimental condition is in the weak collision regime $L > \lambda_i \gg \lambda_D$, where L is either the density scalelength or the dimension of the setup.

3. Results and discussions

3.1. Overall potential distribution

Figure 2 shows the axial variations of the plasma potential with the distance from the small meshes biased at $V_m = -40$ V with respect to the common ground. Obviously the sheath region is reduced with the high geometrical transparency of the mesh, but different meshes almost coincide in presheath profiles. This feature can qualitatively be understood as follows. If the meshes totally absorb the ions, the usual ion sheaths build up on both sides of the negatively biased meshes. However, since the meshes are partially transparent, the ions streaming towards the mesh on one side can partially traverse through the mesh and enter into the sheath on the other side, adding to the ion density there. The larger the geometrical transparency, the higher the ion density is in the sheath. Thus, for the same bias voltage, the electric field is stronger near the mesh with the larger geometrical transparency, which results in the narrowing of the sheath region.

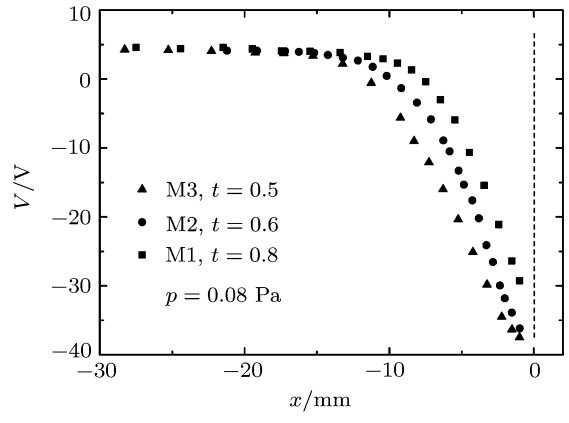


Fig. 2. Potential profiles near three different meshes biased at -40 V with respect to the ground. The vertical dashed line at $x = 0$ represents the location of the mesh.

The thickness of the Child–Langmuir sheath can approximately be estimated by the Child–Langmuir law. Neglecting the electrons in the Child–Langmuir sheath and accounting for the transmitted ions from the other side of the mesh, the Poisson equation can roughly be written as

$$d^2V/dx^2 = -e(1+t)n_i/\varepsilon_0, \tag{1}$$

where t is the transmission coefficient of the mesh, e and n_i are the electronic charge and ion density, respectively, and ε_0 is the vacuum dielectric constant. It is obvious that x scales with $(1+t)^{-1/2}$. Therefore, the sheath thickness is reduced roughly by a factor of $(1+t)^{1/2}$. The estimation gives the ratio of the sheath thickness among the three meshes $1 : 1.06 : 1.1$. Experimentally, the Child–Langmuir sheath can be regarded as starting at the point $n_e/n_i \leq 1\%$.[42] The experimentally measured thicknesses of the Child–Langmuir sheath are 5.3, 6.9, and 9.0 mm, respectively, for the three meshes, corresponding to the ratio $1 : 1.3 : 1.7$. Thus, a qualitative agreement is obtained between the rough estimation and the experimental data but more elaborate model is required to account for the contribution of the transmitted ions.

3.2. Presheath potential drop

Since the measured presheath profiles are almost unchanged for the different meshes except for the shift of the sheath-presheath edge, the presheath regions are essentially governed by the same set of equations. It is generally accepted that the Bohm sheath begins at the point where the ion velocity equals the Bohm velocity. In a collisionless presheath, it is well known that the potential drop is $T_e/2e$. But in a collsional presheath the potential drop depends on the neutral gas pressure since the ions have to overcome the collisional friction. The presheath potential drop can be calculated with the fluid equations

$$n_e = n_{e0} \exp\left(\frac{eV}{T_e}\right), \tag{2}$$

$$\frac{d(n_i v_i)}{dx} = \nu_{ion} n_e, \tag{3}$$

$$m_i \frac{d(n_i v_i^2)}{dx} = -e n_i \frac{dV}{dx} - \nu_i m_i n_i v_i, \tag{4}$$

$$\frac{d^2V}{dx^2} = \frac{e}{\varepsilon_0}(n_e - n_i), \tag{5}$$

where n_e and n_{e0} are the electron density in the presheath and in the bulk plasma, respectively, v_i is the ion velocity, ν_i is the effective ion collision frequency which is mainly due to the ion-neutral charge exchange collisions, and ν_{ion} is the electron impact ionization rate given by

$$\nu_{ion} = n_n \bar{v_e} C_I (I + 2T_e) \exp(-I/T_e), \tag{6}$$

where n_n is the number density of neutral gas, $\bar{v_e}$ is the mean velocity of the electrons, $C_I = 2\times10^{-17}$ cm^2/eV for Ar gas, and $I = 15.8$ eV is the ionization energy.[47]

To calculate the presheath potential drop, the conditions at the boundary of the bulk plasma and the presheath were first determined experimentally. The bulk plasma density n_{e0} and electron temperature T_e were diagnosed by the cylindrical probe, while the potential V was measured by the emissive probe. The ion flow velocity (here is the diffusion velocity) was determined with the method of the phase velocities of two counter propagating ion-acoustic waves.[43] With these input parameters, equations (2)–(5) were numerically solved until the ion velocity reached the Bohm speed. The typical potential drops in the presheath under three different pressures are $\Delta V = 1.4T_e/e$ for $p = 1.5\times10^{-1}$ Pa, $\Delta V = 1.2T_e/e$ for $p = 8\times10^{-2}$ Pa, and $\Delta V = 1.0T_e/e$ for $p = 3.6\times10^{-2}$ Pa, respectively. It is obvious that the potential drop increases with the neutral pressure since it is needed to accelerate the ions to overcome the collisional energy loss.

3.3. Electric field at Bohm sheath edge

With the calculated presheath potential drop, the electric field at the position of the Bohm sheath edge can experimentally be determined from the overall potential distribution. The experimentally measured electric field E_s at the Bohm sheath edge for the cases of three different meshes under a fixed pressure $p = 0.08$ Pa, together with two characteristic electric fields from theoretical models[6,25] are presented in Fig. 3. It is shown that the values of E_s for the three meshes are close to each other, implying that the influence of the transmitted ions on the electric field in the transition region is insignificant. The measured E_s is higher than the electric field in Riemann's transition region $T_e/e\lambda_{Ds}^{3/5}\lambda_i^{2/5}$,[6] but is close to Franklin's result $T_e/e\lambda_{Ds}^{4/5}\lambda_i^{1/5}$.[25] This is in contrast with the result in the case of the sheath near a solid metal plate[33,42] in which the edge electric field is in agreement with that of Riemann's transition region. However, the experimental data also show that E_s is almost not affected by the potential drop V_0-V_m between the bulk plasma and the mesh. The reason is that, with the increase of the potential drop, the plasma can adjust itself to widen the sheath region simply by shifting the Bohm sheath edge toward the plasma side, thus keeping the edge electric field unchanged.

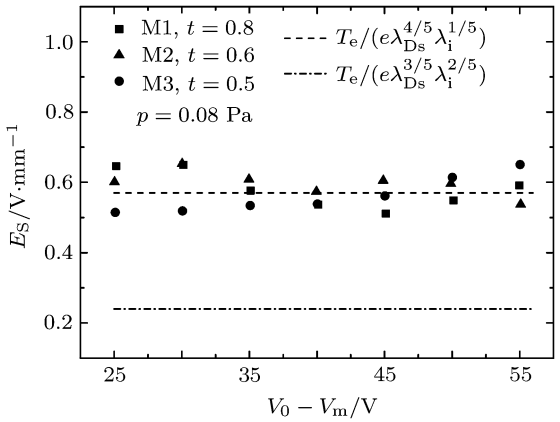


Fig. 3. Variations of the electric field at the Bohm sheath edge with respect to the potential drop $V_0 - V_m$ between the bulk plasma and meshes. Squares, triangles and circles are the experimental data for the meshes M1, M2, M3, respectively, and the dashed and dash-dotted lines are the values from the models of the transition region.

Figure 4 shows the variations of the measured E_s with respect to $V_0 - V_m$ in the sheath of one of the meshes (M3) under different gas pressures (squares: $p = 0.036$ Pa, triangles: $p = 0.080$ Pa, and dots: $p = 0.15$ Pa). The electric field E_s under $p = 0.036$ Pa is much weaker than that under $p = 0.08$ and $p = 0.15$ Pa, while those under $p = 0.08$ and $p = 0.15$ Pa are very close (approximately 0.5 V/mm). This might be understood qualitatively by the ratio of the ion mean-free-path λ_i to the electron Debye length λ_D, which characterize the spatial scales of the presheath and sheath. The values of λ_i/λ_D under $p = 0.15$ and 0.080 Pa are 130 and 140 respectively, while the value under $p = 0.036$ Pa is 190, which is much greater than that under the other two pressures. This means that

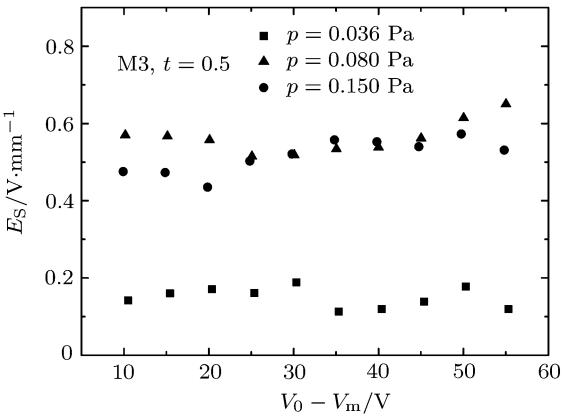


Fig. 4. Variations of the electric field at the Bohm sheath edge with respect to the potential drop $V_0 - V_m$ between the bulk plasma and the mesh M3 under different pressures.

the ions under higher pressures need stronger electric fields to be accelerated to the Bohm velocity in the presheath. To see the effect in more details, we compare in Table 1 the measured E_s with several characteristic electric fields in the transition region from Refs. [6] and [25]. It is shown that at the lower pressure the experimental E_s at the Bohm sheath edge is close to Riemann's result $T_e/e\lambda_{Ds}^{3/5}\lambda_i^{2/5}$,[6] while at the higher pressure the experimental E_s is close to Franklin's result $T_e/e\lambda_{Ds}^{4/5}\lambda_i^{1/5}$.[25] The theoretically calculated edge electric field E_s^{th} based on the one-dimensional fluid equations is close to T_e/λ_i, which is much smaller than the experimental E_s. Thus, the simple fluid model underestimates the edge electric field since the contribution of the transmitted ions is not included.

Table 1. Comparison of the measured electric field $E_{s,M1}$, $E_{s,M2}$, and $E_{s,M3}$ at the Bohm sheath edge near the meshes M1, M2, and M3 and under three pressures with the electric fields from the models of the transition region and the edge electric field E_s^{th} calculated from Eqs. (2)–(6). The meshes were biased at −20 V. The unit for the electric fields is V/mm.

p/Pa	$E_{s,M1}$	$E_{s,M2}$	$E_{s,M3}$	$T_e/e\lambda_{Ds}^{3/5}\lambda_i^{2/5}$	$T_e/e\lambda_{Ds}^{4/5}\lambda_i^{1/5}$	$T_e/e\lambda_i$	E_s^{th}
0.036	0.20	0.22	0.16	0.19	0.48	0.011	0.020
0.080	0.65	0.60	0.51	0.24	0.57	0.018	0.031
0.15	0.71	0.56	0.50	0.24	0.54	0.022	0.038

3.4. Bohm sheath thickness

Using the presheath potential drop determined in Subsection 3.2, the position of the sheath-presheath edge and thus the thickness of the Bohm sheath can experimentally be determined. In addition, according to the measured electric field E_s at the Bohm sheath edge, the Bohm sheath thickness can also be calculated by numerically solving Eqs. (2)–(5).

Figure 5 shows the variations of the experimentally measured and theoretically calculated Bohm sheath thickness with respect to the potential drop between the bulk plasma V_0 and the mesh V_m in the case of a fixed mesh (M2) but under different neutral pressures. Since the plasma parameters vary with the pressure, the thickness is normalized by λ_D, while the potential drop is normalized by T_e/e. It is shown that both the experimental and the theoretical sheath thickness increase along with the potential drop. However, the normalized thickness is reduced if the pressure is raised. In the low pressure case when $p = 3.6 \times 10^{-2}$ Pa, the experimental sheath thickness can be as large as a few tens of Debye lengths, but in the high pressure case when $p = 1.5 \times 10^{-1}$ Pa, it is only about several to a little more than 10 Debye lengths. Since plasmas under these pressures are weakly collisional, the sheath region is essentially collisionless. Thus, the decrease of the normalized thickness with the increase of the pressure might be related to the asymmetry of the sheaths on the two sides of the mesh, which needs further investigation but is beyond the scope of this paper. It is noted that under relatively high pressures, the theoretical thickness (dotted curve) fits well to the experimental data (circles). However, under low pressures, there is a big discrepancy between the theoretical curve (solid line) and experimental data (squares). One of the reasons for the discrepancy is that the theoretical model is for the idealized absorbing walls which does not account for the partially transparent boundaries. Another effect might be the flow of the bulk plasma which depends on the gas pressure but is lacking the modeling. Thus, much more sophisticated model is needed to explain the experimental results.

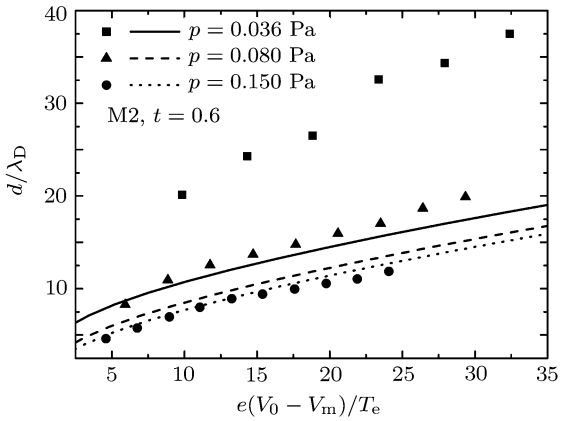


Fig. 5. Variations of the normalized sheath thickness d/λ_D near the mesh M2 with respect to the normalized potential drop $e(V_0 - V_m)/T_e$. Squares, triangles, and circles are the experimental data for $p = 3.6\times10^{-2}$, 8×10^{-2}, and 1.5×10^{-1} Pa, respectively. Solid, dashed, and dotted lines are the theoretical curves for $p = 3.6 \times 10^{-2}$, 8×10^{-2}, and 1.5×10^{-1} Pa, respectively.

Under a fixed pressure, figure 6 shows the varia-

tions of the measured thickness of the Bohm sheath near different meshes together with the theoretical curve calculated from Eqs. (2)–(6) (solid line) with respect to the potential drop ($V_0 - V_m$). It is shown that the thickness for the mesh M1 ($t = 0.8$) is appreciably smaller than that for the other two meshes. The overall variations of d are in qualitative agreement with the theoretical curve, but the theoretical values of d are systematically greater than the experimental ones. The difference between the experiment and theory is reduced when the transmission coefficient of the mesh is decreased. The discrepancy is partially because the effect of the transmitted ions is not involved in the simple one-dimensional fluid model.

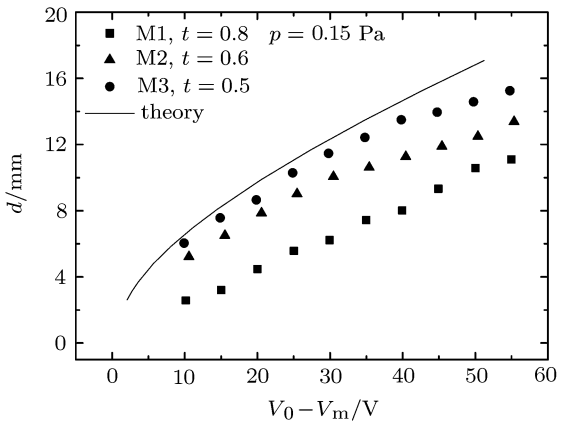


Fig. 6. Variations of the thickness d of the Bohm sheath near different meshes with respect to the potential drop $V_0 - V_m$ under a fixed pressure. Squares, triangles, and circles are the experimental data for M1, M2, and M3, respectively, and solid line is the theoretical curve.

4. Conclusion

The potential distributions in the sheath and presheath regions near meshes of different transmissivity under different neutral gas pressures were measured with a fine structured emissive probe in the modified double-plasma device. The measured sheath thickness and electric field were compared with theoretical models. It is shown that, because of the partial transmission of the ions, the sheath region becomes narrower and the electric field in the sheath is stronger for the mesh of higher transmissivity, owing to the increase of the ion density in the sheath region contributed from the ions transmitted from the other side of the mesh. However, the presheath potential profiles remain almost the same for different meshes because of the self-adjustment of the plasma except the shift of the sheath-presheath edge. The thickness of the Bohm sheath decreases while the electric field at the Bohm sheath edge increases with the increase of the pressure. Under the relatively high pressure, there is a good agreement between the measured and the calculated sheath thicknesses, while under the low pressure, there is a big discrepancy between the experimental and theoretical results. Furthermore, the measured edge electric field under low pressure is close to Riemann's model of the transition region,[6] while that under high pressure is close to Franklin's result.[25] The calculated values of the electric field at the Bohm sheath edge based on the one-dimensional fluid equations for absorbing walls are much lower than the experimental data, which indicates that elaborate models for the sheath structures near partially transmitting meshes need future investigations.

References

[1] Tonks L and Langmuir I 1929 *Phys. Rev.* **34** 876
[2] Hershkowitz N 2005 *Phys. Plasmas* **12** 055502
[3] Allen J E 2009 *Plasma Sources Sci. Technol.* **18** 014004
[4] Franklin R N 2003 *J. Phys.* D **36** R309
[5] Riemann K U 1991 *J. Phys.* D **24** 493
[6] Riemann K U 1997 *Phys. Plasmas* **4** 4158
[7] Yu M Y, Saleem H and Luo H 1992 *Phys. Fluids* B **4** 3427
[8] Ma J X, Liu J Y and Yu M Y 1997 *Phys. Rev.* E **55** 4627
[9] Dai Z L, Wang Y N and Ma T C 2001 *Acta Phys. Sin.* **50** 2398 (in Chinese)
[10] Liu J Y, Wang Z X and Wang X 2003 *Phys. Plasmas* **10** 3032
[11] Wang Z X, Liu J Y, Zou X, Liu Y and Wang X G 2004 *Acta Phys. Sin.* **53** 793 (in Chinese)
[12] Zou X, Liu J Y, Wang Z X, Gong Y, Liu Y and Wang X G 2004 *Acta Phys. Sin.* **53** 3409 (in Chinese)
[13] Wang J L, Zhang G L, Liu Y F, Wang Y N, Liu C Z and Yang S Z 2004 *Chin. Phys.* **13** 65
[14] Li Y F and Ma J X 2006 *Phys. Plasmas* **13** 013501
[15] Duan P, Liu J Y, Gong Y, Zhang Y, Liu Y and Wang X G 2007 *Acta Phys. Sin.* **56** 7090 (in Chinese)
[16] Zou X, Liu H P and Gu X E 2008 *Acta Phys. Sin.* **57** 5111 (in Chinese)
[17] Liu C S, Wang D Z, Liu T W and Wang Y H 2008 *Acta Phys. Sin.* **57** 6450 (in Chinese)
[18] Wang D Y, Ma J X, Li Y R and Zhang W G 2009 *Acta Phys. Sin.* **58** 8432 (in Chinese)
[19] Yu D, Zhang F, Liu H, Li H, Yan G and Liu J 2008 *Phys. Plasmas* **15** 104501
[20] Gong Y, Wang X, Duan P, Yu J and Wang D 2005 *Phys. Plasmas* **12** 043501

[21] Dai Z L, Xu X and Wang Y N 2007 *Phys. Plasmas* **14** 013507
[22] Godyak V and Sternberg N 2002 *Phys. Plasmas* **9** 4427
[23] Hutchinson I H 2002 *Phys. Plasmas* **9** 1832
[24] Franklin R N and Snell J 2001 *Phys. Plasmas* **8** 643
[25] Franklin R N 2004 *J. Phys.* D **37** 1342
[26] Benilov M S 2000 *IEEE Trans. Plasma Sci.* **28** 2207
[27] Kono A 2003 *Phys. Plasmas* **10** 4181
[28] Lonngren K E and Alexeff I 2008 *Phys. Plasmas* **15** 093505
[29] Bohm D 1949 *The Characteristics of Electrical Discharges in Magnetic Fields* ed. Guthrie A and Wakerling R K (New York: McGraw-Hill) p. 77
[30] Goeckner M J, Goree J and Sheridan T E 1992 *Phys. Fluids* B **4** 1663
[31] Oksuz L, Khedr M A and Hershkowitz N 2001 *Phys. Plasmas* **8** 1729
[32] Severn G D, Wang X, Ko E and Hershkowitz N 2003 *Phys. Rev. Lett.* **90** 145001
[33] Oksuz L and Hershkowitz N 2002 *Phys. Rev. Lett.* **89** 145001
[34] Crawford F W and Cannara A B 1965 *J. Appl. Phys.* **36** 3135
[35] Goldan P D 1970 *Phys. Fluids* **13** 1055
[36] Annaratone B M, Antonova T, Thomas H M and Morfill G E 2004 *Phys. Rev. Lett.* **93** 185001
[37] Lonngren K E, Khazei M, Gabl E F and Bulson J M 1982 *Plasma Phys.* **24** 1483
[38] Klostermann H, Rohde A and Piel A 1997 *Phys. Plasmas* **4** 2406
[39] Nakamura Y, Bailung H and Lonngren K E 1999 *Phys. Plasmas* **6** 3466
[40] Li Y F, Ma J X, Li Y R, Xiao D L and Lonngren K E 2006 *Phys. Lett. A* **358** 297
[41] Xiao D L, Ma J X, Li Y R, Li Y F and Yu M Y 2007 *Phys. Plasmas* **14** 092104
[42] Li Y R, Ma J X, Wang D Y and Zhang W G 2008 *J. Phys.* D **41** 225210
[43] Ma J X, Li Y F, Xiao D L, Li J J and Li Y R 2005 *Rev. Sci. Instrum.* **76** 062205
[44] Smith J R, Hershkowitz N and Coakley P 1979 *Rev. Sci. Instrum.* **50** 210
[45] Wang X and Hershkowitz N 2006 *Rev. Sci. Instrum.* **77** 043507
[46] Sheldon J W 1962 *Phys. Rev. Lett.* **8** 64
[47] Raizer Y P 1997 *Gas Discharge Physics* (Berlin: Springer) p. 53